Multi-generation Chemical Aging of α-Pinene Ozonolysis Products by Reactions with OH

N. Wang[1], E. Kostenidou[2,3], N. M. Donahue[1] and S. N. Pandis[1,2,3]

[1]Department of Chemical Engineering, Carnegie Mellon University, Pittsburgh, US

[2]Department of Chemical Engineering, University of Patras, Patra, Greece

[3] Institute of Chemical Engineering Sciences (ICE-HT), FORTH, Patra, Greece

Abstract

Secondary organic aerosol (SOA) formation from volatile organic compounds (VOCs) in the atmosphere can be thought of as a succession of oxidation steps. The production of later-generation SOA via continued oxidation of the first-generation products is defined as chemical aging. This study investigates aging in the α-pinene ozonolysis system with hydroxyl radicals (OH) through smog chamber experiments. The first-generation α-pinene ozonolysis products were allowed to react further with OH formed via HONO photolysis. After an equivalent of 2-4 days of typical atmospheric oxidation conditions, homogeneous OH oxidation of the α-pinene ozonolysis products resulted in a 20-40 % net increase of the SOA for the experimental conditions used in this work. A more oxygenated product distribution was observed after aging based on the increase in aerosol atomic oxygen to carbon ratio (O:C) by up to 0.04. Experiments performed at intermediate relative humidity (RH) of 50 % showed no significant difference in additional SOA formation during aging compared to those performed at low RH of less than 20 %.

1. Introduction

Anthropogenic activities such as fuel combustion as well as biogenic sources such as emissions from vegetation can introduce particles and particle precursors into the atmosphere. In most areas, about half of the submicron aerosol mass on average is composed of organic compounds (Zhang et al., 2007). Organic particles directly emitted to the atmosphere are traditionally defined as primary organic aerosol (POA), while those formed through atmospheric

29 reactions and condensation of species with corresponding volatility are secondary (SOA).

30 Atmospheric aerosols represent a significant risk to human health by causing respiratory problems

31 and heart attacks (Davidson et al., 2005; Pope et al., 2009). At the same time these particles

32 influence the climate of our planet (Intergovernmental Panel on Climate Change, 2007).

33 Oxygenated OA with a high oxygen to carbon ratio (O:C) is often the most important

34 component of ambient OA suggesting the importance of atmospheric chemistry in the formation

35 and processing of OA (Zhang et al., 2007). Early studies of SOA formation (Grosjean and Seinfeld,

36 1989; Izumi and Fukuyama, 1990; Odum et al., 1996) focused on the first stage of reactions

37 involving the target precursor reacting with the chosen oxidant. In the atmosphere, organic vapors

38 and particles interact with oxidants for days and therefore successive oxidation processes are

39 inevitable.

40 Chemical aging refers to the subsequent stages of SOA formation and evolution due to the

41 production of later-generation products via oxidation of first-generation products by oxidants such

42 as OH free radicals (Donahue et al., 2006; Henry et al., 2012). Previous studies have explored

43 various forms of aging, including heterogeneous reactions of oxidants and aerosols (George et al.,

44 2008), oligomerization (Kalberer et al., 2006), photolysis of either gas or condensed-phase

45 products (Henry and Donahue, 2012), and homogeneous gas-phase oxidation by OH (Donahue et

46 al., 2012). Homogeneous gas-phase oxidation reactions appear to be in general much faster than

47 heterogeneous reactions, due to diffusion limitations of the latter (Lambe et al., 2009). The first-

48 generation oxidation reactions of most SOA precursors convert much less than 50 % of the

49 precursor to SOA, leaving more than half of the carbon still in the gas-phase. Additional oxidation

50 of these vapors can potentially contribute additional and more oxygenated SOA components.

51 These later-generation reactions have been proposed to be a major missing step connecting

52 chamber studies to field measurements.

53 Zeroth order parameterizations have been developed to model the chemical aging of semi-

54 volatile POA emissions in chemical transport models (Robinson et al., 2007). CTMs using these

55 schemes show improved performance in urban areas such as Mexico City (Tsimpidi et al., 2011),

56 but tend to over-predict OA in areas such as the southeastern United States where biogenic VOCs

57 dominate if chemical aging is assumed to be a major source of additional SOA (Lane et al., 2008).

58 As a result, the importance of aging of biogenic SOA as a source of SOA mass concentration

59 remains an issue of debate.

The ozonolysis of α-pinene ($C_{10}H_{16}$) is considered one of the most important global SOA sources (Griffin et al., 1999). The system has been well characterized through smog chamber experiments where researchers quantified its SOA yields under different conditions, explored the reaction pathways and mechanisms, and identified its product distributions. Recent studies suggest that there is significant potential for additional SOA formation from homogeneous gas-phase aging by OH of the first-generation α-pinene oxidation products (Donahue et al., 2012; Müller et al., 2012; Chacon-Madrid et al., 2013). Major identified products existing in gas phase such as pinonaldehyde and pinonic acid can serve as SOA precursors and further react with OH. Pinonaldehyde reacts with OH, with SOA mass yields up to 5 % under low-NO_x conditions and 20 % under high-NO_x conditions (Chacon-Madrid et al., 2013). Müller et al. (2012) demonstrated the formation of 1,2,3-butanetricarboxylic acid (MBTCA), an SOA product of low volatility identified in α-pinene ozonolysis, through the gas-phase OH oxidation of pinonic acid. They reported an experimental yield of 0.6 % for MBTCA from the gas-phase OH oxidation of pinonic acid, accounting for about 10 % of the total SOA formed. The proposed formation mechanisms of MBTCA is a classic example of semi-volatile precursors going through oxidation and forming products of lower volatility.

The Multiple Chamber Aerosol Chemical Aging Study (MUCHACHAS) explored the gas-phase OH aging effects of the α-pinene ozonolysis products via experiments performed in four different smog chambers (Donahue et al., 2012). They were able to isolate the aging effect by using different OH sources (HOOH photolysis, HONO photolysis, TME ozonolysis), light sources (sunlight, quasi-solar lamps, 350 nm UV lamps), and chambers of different design in size and material (Teflon and aluminum). Almost in all experiments, additional formation of SOA (up to 55 %) and a more oxidized product distribution (increasing O:C) were observed after aging. However, in one of the chambers, strong UV photolysis led to decreasing SOA mass concentrations in experiments with low to moderate OH levels, $[OH] \leq 2 \times 10^6$ molecules cm^{-3} (Henry and Donahue, 2012). These authors concluded that chemical aging involves a complex set of interacting processes with competing functionalization (conserved C number with products of lower volatility and higher oxidation states) and fragmentation (cleavage of C-bond with products over a wide volatility range and higher oxidation states) of the various organic compounds. A 2D-volatility basis set (2D-VBS) simulation based on these two pathways and a branching ratio between them showed that homogeneous OH aging can potentially more than double the α-pinene

SOA mass concentration, after about a day's equivalent of typical atmospheric oxidation conditions. Uncertainties such as "ripening" during which SOA volatility evolves but its mass remains constant, UV photolysis and heterogeneous OH uptake can further complicate the aging process.

Qi et al. (2012) also explored aging of the α-pinene ozonolysis system through smog chamber experiments using HOOH as an OH source and studied the UV photolysis effect. They observed a 7.5 % increase in the SOA volume concentration and an increase of 0.03 in the O:C after aging. Minimum photolysis effect was reported for these experiments.

One complication of chamber experiments is the interaction of particles with chamber walls. The wall-loss rate of particles is a function of particle size, charge distribution, chamber geometry, turbulence, and electric field within the chamber (Crump and Seinfeld, 1981). In order to quantify SOA yields from chamber experiments, it is important to correct for particle wall loss. Recent findings that organic vapors in the chamber can be directly lost to the Teflon walls as well further complicate the wall-loss correction process (Matsunaga and Ziemann, 2010; Zhang et al., 2014). Krechmer et al. (2016) measured the loss rate of vapors formed in the chamber and found the corresponding timescale to be 7-13 min. Ye et al. (2016) determined the vapor wall-loss timescale in the Carnegie Mellon chamber used in this work to be around 15 min for semi-volatile organic compounds.

Despite the consensus from the aforementioned chamber studies that gas-phase OH aging of α-pinene ozonolysis products can contribute to additional SOA formation, there lacks consistency in the extent to which the additional mass can form for different OH exposures. Part of the problem is that the estimated amount of additional SOA formed from these long-lasting aging experiments can be extra sensitive to the particle and the vapor wall-loss correction methods deployed. The uncertainties at the end of a 10-hour long aging experiment during which most particles are lost to chamber walls and the measured suspended mass is low can be relatively high. In this work, we aim to quantify the additional SOA formed during the aging step comparing measurements from a suite of instrumentation. We adopt a size-dependent particle wall-loss correction method and develop a procedure to better constrain the associated errors. We also attempt to constrain the vapor loss using both theoretical calculations and measurements.

2. Experimental approach

We conducted experiments in a 12 m^3 Teflon (Welch Fluorocarbons) smog chamber at Carnegie Mellon University (CMU). The reactor was suspended in a temperature-controlled room with walls covered with UV lights (GE 10526 and 10244). Prior to each experiment, we flushed the chamber overnight with purified air under UV illumination to remove any residual particles and gas-phase organics. We generated purified air by passing ambient air through a high-efficiency particulate air (HEPA) filter to remove particles, an activated carbon filter to remove any organics, a Purafil filter to remove NO_x, and finally a silica gel filter, keeping relative humidity (RH) below 5 % in the chamber before each experiment.

We pumped an ammonium sulfate solution (1 g L^{-1}) into the chamber at the beginning of each experiment through an atomizer (TSI, model 3076) at a constant rate of 90 mL h^{-1} to produce droplets. The droplets passed through a diffusion dryer and a neutralizer to produce dry ammonium sulfate seed particles. We injected seeds with a number mode size of 110 nm until they reached a number concentration of 2×10^4 cm^{-3}, resulting in an initial seed mass concentration of around 40 μg m^{-3} and a surface area concentration of up to 1000 μm^2 cm^{-3}. Typical organic vapors with a molar weight of 250 g mol^{-1} thus had an initial collision frequency with these seeds of 0.01 s^{-1}. We injected α-pinene (Sigma-Aldrich, ≥ 99 %) into the chamber using a septum injector with purified air as carrier flow. We generated ozone using a corona-discharge ozone generator (AZCO, HTU500AC) to initiate the ozonolysis reaction. We prepared a fresh HONO solution in a bubbler by adding a 4.9 g L^{-1} sulfuric acid solution to a 6.9 g L^{-1} sodium nitrite solution. We then turned on the UV lights to start the photo-dissociation of HONO, producing OH.

At the end of each experiment, we injected additional ammonium-sulfate seeds into the chamber using the same method with a more concentrated solution (5 g L^{-1}) in order to characterize the particle wall-loss rates a second time.

We added butanol-d9 (Cambridge Isotope Laboratories, 98 %) into the chamber through the septum injector as an OH tracer before the reaction started and used the method described in Barmet et al. (2012) to calculate the OH produced by HONO photolysis. The OH concentration in these experiments was around 2.4×10^7 molecules cm^{-3} for the first hour, then dropped to around 5×10^6 molecules cm^{-3} afterwards. The introduction and photolysis of HONO produces hundreds of ppb of NO_x, and thus the aging reactions in this work occurred under high NO_x conditions; the majority of the peroxy radicals reacted with NO during the aging phase of the experiments.

153   We performed experiments at both low RH of less than 20 % and intermediate RH of 50 %.

154 To add water vapor to the chamber, we used a stream of purified air to carry ultrapure water

155 (Millipore water purification system) in a bubbler into the chamber before the introduction of seeds.

156   We measured the particle size distribution using a TSI Scanning Mobility Particle Sizer,

157 SMPS (classifier model 3080; CPC model 3010 or 3772), with flows adjusted to measure particle

158 diameters in the 15-700 nm range. We measured the particle composition and mass spectrum of

159 the OA with an Aerodyne High Resolution Time-of-flight Aerosol Mass Spectrometer (HR-Tof-

160 AMS). We monitored the concentrations of α-pinene and butanol-d9 using a Proton Transfer

161 Reaction-Mass Spectrometer (PTR-MS, Ionicon), the ozone concentration using a Dasibi 1008

162 ozone monitor (ICE: Teledyne 400E), and NO_x (NO + NO_2) levels using a Teledyne API NO_x

163 Analyzer 200A (ICE: Teledyne T201). We held the chamber temperature constant at 22 ºC

164 throughout all experiments. We list the initial conditions of the experiments performed for this

165 work in Table 1.

166

167 **3. Data analysis**

168 **3.1 SOA yields**

169   The SOA mass yield, Y, is a metric of the ability of a gaseous precursor to form SOA, and

170 is defined as $Y= C_{SOA}/\Delta VOC$, where C_{SOA} is the produced SOA mass concentration (in μg m^{-3})

171 and ΔVOC the amount of the VOC precursor (α-pinene in this case) reacted (in μg m^{-3}). To

172 separate the effect of aging on SOA mass concentration, we define a first-generation SOA mass

173 yield, $Y_1= C_{SOA,1}/\Delta VOC$, and a second-generation SOA mass yield, $Y_2= C_{SOA,2}/\Delta VOC$. $C_{SOA,1}$ and

174 $C_{SOA,2}$ are the concentrations of SOA formed before, and after aging with hydroxyl radicals. All

175 α-pinene reacts away during the first stage and thus ΔVOC for the second stage is the same as the

176 initial α-pinene concentration in the chamber.

177

178 **3.2 Particle wall-loss correction**

179   In this work, we try to reduce the uncertainties in the estimated SOA mass concentration

180 associated with the particle wall-loss correction. This uncertainty can be significant due to two

181 aspects of these aging experiments: the evolution of the particle size distribution and the duration

182 of the experiments. In these aging experiments, where particles grow by condensation and

183 coagulation for several hours, the particle size distribution can potentially shift, covering a wide

size range over the course of an experiment. Particle wall losses are size dependent, and this shift can introduce significant errors if a constant loss rate constant is assumed. To minimize these problems, we adopted a size-dependent particle wall-loss correction method where we determined the particle wall-loss rate constant, k, at each particle size, D_p.

3.2.1 Determination of particle wall-loss rate constants

The size-dependent particle wall-loss correction method (Keywood et al., 2004; Ng et al., 2007; Loza et al., 2012; Nah et al., 2016) adopted in this work is based on the SMPS-measured particle size distribution. At each particle size bin i, the first-order particle wall-loss rate constant k, can be determined as the slope of the following equation:

$$\ln[N_i(t)] = -k_i t + Q \tag{1}$$

where $N_i(t)$ is the SMPS-measured aerosol number concentration at size bin i and Q is an arbitrary constant. Applying Eqn. 1 across the entire SMPS-measured particle size range, we obtain the particle wall-loss rate constant function, $k(D_p)$.

To determine the $k(D_p)$ profile, we utilized the initial four-hour ammonium sulfate seed wall-loss period for each experiment. Since k may also vary with time (McMurry and Rader, 1985), we determined a second $k(D_p)$ profile for each experiment using the ammonium sulfate seed wall-loss period at the end. It is important to ensure that the k's, especially at sizes where the majority of SOA mass is distributed, remain the same over the course of each experiment.

The $k(D_p)$ values calculated (with an $R^2 > 0.5$) based on SMPS measurements of the seed distribution from this work usually only cover particle size range of 30-300 nm due to the lack of particles at either end of the particle size distribution. To determine the $k(D_p)$ for $D_p < 30$ nm, we use a simple log-linear fit of k's from 30-50 nm and back extrapolate it to 10 nm. To determine $k(D_p)$ for $D_p > 300$ nm, we assume that the constant is practically the same in the 300-700 nm range. We confirmed this with additional seed-only experiments where there were enough particles at that size range (Wang et al., 2017). Significant increases of the rate loss constant are observed for particles larger than 1 μm, while in our experiments the particles remained small than 600 nm or so. A measure of the uncertainty of these corrections is the variability of the corrected mass concentration during the seed wall-loss periods as discussed in the next section. Details regarding

215   the wall-loss profiles in the CMU chamber and the execution of the size-dependent particle wall-

216   loss correction for this work can be found in Wang et al. (2017).

217

218   **3.2.2 Correction of SMPS measurements**

219   The corrected particle number concentration at each size bin i, $N_i(t)$, can be calculated

220   numerically,

221

222    $$N_i(t) = \mathrm{N}_i^m(t) + k_i \int_0^t \mathrm{N}_i^m(t)dt, \qquad (2)$$

223

224   from the measured values $\mathrm{N}_i^m(t)$ and the $k(D_p)$ corresponding to the size bin i, k_i.

225   For closed systems in which coagulation is slow, the particle wall-loss corrected number

226   concentration should be constant. In order to evaluate how well the correction works, we define

227   the parameter: $\varepsilon_N = 2\sigma_{N_s}/\overline{N_s}$, where σ_{N_s} is the standard deviation of the particle wall-

228   corrected number concentration for the seed wall-loss periods and $\overline{N_s}$ the average. Similarly, we

229   define $\varepsilon_V = 2\sigma_{N_s}/\overline{V_s}$ based on the particle wall-loss corrected volume concentration for the two

230   seed wall-loss periods. Only when all four values, ε_N and ε_V for both the initial and the final seed

231   periods, are less than 5 % do we deem the particle wall-loss correction valid for that individual

232   experiment. Experiments in which these criteria were not met were not included in the analysis.

233   To calculate the mass concentration of the formed SOA, C_{SOA}, during the course of an

234   experiment, we treated the particle wall-loss corrected aerosol volume concentration $V(t)$

235   differently before and after its maximum, V_{max} . For

236

237    $$\mathrm{t} < t_{V_{max}}, C_{SOA}(t) = (V(t) - V_s)\rho_{SOA},$$

238    $$\mathrm{t} \geq t_{V_{max}}, C_{SOA}(t) = [V(t) - V_s\frac{V(t)}{V_{max}}]\rho_{SOA}, \qquad (3)$$

239

240   where $t_{V_{max}}$ is the corresponding time at the maximum particle wall-loss corrected total aerosol

241   volume concentration. V_s is the average particle wall-loss corrected seed volume concentration

242   before the beginning of each experiment. ρ_{SOA} is the SOA density, assumed to be equal to 1.4 µg

243   m^{-3} (Kostenidou et al., 2007). Ideally, $V(t)$ should equal to V_{max} after the reactions are completed

244   and particle wall loss is the only process after $t_{V_{max}}$. However, deviations of $V(t)$ from V_{max} are

245 caused by the uncertainty associated in applying the size-dependent wall-loss corrections. By

246 scaling V_s with $V(t)/V_{max}$, we are distributing the impact of any potential fluctuations in $V(t)$ evenly

247 to both the seeds and the organics, and thus obtain a more stable C_{SOA} after aging.

248

249 **3.3 Analysis of AMS measurements**

250 The HR-AMS was operated in V mode during the experiments in this work. Squirrel v1.56D was

251 used to analyze the data. The atomic oxygen to carbon ratio, O:C, was determined based on the

252 unit-resolution correlation described in Caragaratna et al. (2015). Nitrate signals were attributed

253 to organics since the only sources of them in these experiments are organonitrates.

254   In an attempt to explore the functionalities/products that may have changed during aging,

255 we used the AMS high-resolution (HR)family analysis. We used Pika 1.15D to analyze the HR

256 data. Each fitted ion is grouped into a "family" based on their chemical formula, and the families

257 used are: CH, CHO, CHO_2, C_x, HO, and NO. These are the main components of the organics

258 formed, with family HO calculated by subtracting the concentrations of the other families from the

259 total organic signal. This is necessary because the fragmentation of sulfates can interfere with the

260 family HO. Family NO can be used to represent the organonitrates formed during the aging phase

261 of the experiments.

262

263 **4. Results and discussion**

264   The particle wall-loss corrected aerosol number concentration evolution during a typical

265 experiment (Exp. 1) together with the SMPS raw measurements are shown in Fig. 1. Prior to the

266 ozonolysis, 18,000 cm^{-3} ammonium sulfate particles were added to the chamber as seeds. After a

267 4.5 h wall-loss period, 8,000 cm^{-3} particles remained suspended, serving as pre-existing surface

268 for condensation. At t=0, ozone was added into the chamber, reacting with α-pinene to form

269 condensable first-generation products. The ozonolysis of α-pinene has been found to produce OH

270 with a molar yield of approximately 0.7 (Paulson et al., 1998), which in our experiments resulted

271 in approximately one third of the precursor reacting with OH. An additional 100 cm^{-3} particles

272 were formed due to nucleation at this time. Two doses of HONO were added into the chamber in

273 this experiment at t=0.4 h and t=1.3 h, respectively. HONO was allowed to mix in the chamber

274 and then the UV lights were turned on at t=0.8 h and t=1.8 h to produce OH. At t=3.5 h, another

275 10,000 cm^{-3} ammonium sulfate particles were added into the chamber for a second 4 h long
276 determination of the $k(D_p)$ profile for this experiment.

277 The two $k(D_p)$ profiles determined from the initial seed wall-loss period and the one at the
278 end of the experiment are shown in Fig. 2. They agree relatively well with small discrepancies at
279 $D_p < 50$ nm. The complete $k(D_p)$ profile used for the size-dependent particle wall-loss correction
280 is also shown.

281 As indicated in Fig. 1, the particle wall-loss corrected aerosol number concentration
282 remains relative level at t<0 h and t>3.5 h, with $\varepsilon_{N,1} = 3.3$ % and $\varepsilon_{N,2} = 0.5$ %, respectively. The
283 particle wall-loss corrected aerosol volume concentration (Fig. 3) at the initial seed wall-loss
284 period and that at the end had variabilities equal to $\varepsilon_{V,initial} = 4.2$ % and $\varepsilon_{V,end} = 3.8$ %,
285 respectively. All parameters were less than 5 % and therefore the accuracy of the wall-loss
286 correction was acceptable.

287 The particle wall-loss corrected aerosol volume concentration evolution for Exp. 1 together
288 with the corresponding SMPS raw measurements are shown in Fig. 3. Particles grew from t=0 to
289 0.7 h and t=0.8 to 1 h due to vapor condensation. The total aerosol volume peaked at t=0.7 h during
290 the first-generation oxidation, and reached its maximum at t=1.1 h due to aging during the second-
291 generation oxidation. The change in volume during the second addition of OH at 1.7 h was
292 negligible.

293 The SOA mass concentration evolution for Exp. 1 calculated using Eqn. 3 is shown in Fig.
294 4. The error bars are calculated using the highest ε (in this case $\varepsilon_{V,1} = 4.2$ %). For this experiment,
295 37.7±1.6 µg m^{-3} of SOA was formed during ozonolysis. An additional 11.1±2.6 µg m^{-3} SOA was
296 formed during the first aging period. The SOA reached 48.8±2 µg m^{-3} after aging and remained
297 approximately constant utill the end of the experiment. The total SOA produced and the calculated
298 SOA yields for all experiments are listed in Table 2.

299 The AMS-derived atomic oxygen to carbon ratio (O:C) evolution for Exp. 1 is shown
300 together with the AMS-measured aerosol composition (assuming CE=1) in Fig. 5. The increase in
301 the sulfate signals at t=0 is caused by a change in the instrument collection efficiency. Due to the
302 uncertainty caused by CE changes over the course of an experiment, we did not use the absolute
303 AMS-measured organic mass concentration for any quantitative analysis. Using the algorithm
304 derived by Kostenidou et al. (2007), we calculated the CE to be ~0.25 for the initial seed period
305 and ~0.4 after the seeds were coated with organics. A quick check comparing the two stepwise

306   increase in the CE-corrected organic mass concentration to those derived from SMPS revealed that

307   the results from both instrument agreed reasonably well. The algorithm also estimated that the

308   SOA density was 1.3 ± 0.15 g cm^{-3} in good agreement with the Kuwata et al. (2012)

309   parameterization based on the measured O:C and H:C which also predicted 1.3 g cm^{-3}.

310   The O:C is a collective measure for the ongoing chemistry during these aging experiments.

311   In Exp. 1, the O:C kept decreasing due to the freshly-formed semi-volatile SOA condensing onto

312   particles from t=0 to 0.5 h. Later during the dark period (t=0.5 h to 0.8 h), the O:C ratio kept

313   decreasing to 0.42 while the organic mass concentration stayed almost constant. This is consistent

314   with the "ripening" phenomenon, first observed during the MUCHACHAS campaign, where the

315   composition of the formed SOA keeps evolving after α-pinene has reacted while the change in

316   SOA mass is minimal (Tritscher et al., 2011). The nature of this process is not well-understood,

317   but it probably involves heterogeneous reactions. After OH radicals were generated in the chamber

318   at t=0.8 h, the semi-volatile vapors got oxidized to form second-generation products of lower

319   volatility, resulting in an increase of 0.02 in O:C in about 10 min. After t=1 h, the O:C remained

320   relatively constant but it started to decrease at t=1.25 h when the UV lights were turned off. Since

321   aging is a complex process that involves functionalization, fragmentation and heterogeneous

322   reactions, the trends in O:C are indicative of the competition among these processes. The decrease

323   we observed here was associated with turning the UV lights off, and thus it is likely that some

324   chemistry was perturbed and thus the processes resulting in decreasing O:C took over. The

325   decrease in O:C associated with turning off the UV lights was not consistent across the five

326   experiments. This further proves that this phenomenon is the result of several competing process

327   and needs further investigation on a molecular level. An inflection point at t=1.7 h was observed

328   after a second dose of OH being introduced in the chamber. Instead of the stepwise increase like

329   the one observed after the first dose of OH, the O:C increased slowly but steadily this time until

330   the end of the experiment to 0.45 with no significant increase in organic mass. This is also quite

331   consistent with what was observed in MUCHACHAS.

332   We used the organic to sulfate ratio (Org/Sulf) derived from AMS measurements to look

333   at the SOA formation in these experiments due to its insensitivity to changes in collection

334   efficiency. The Org/Sulf time series for Exp. 1 is shown in Fig. 6. The ratio increased to 1.25 at

335   t=0.7 h as the result of the first-generation vapors condensing onto pre-existing particles. After we

336   first turned on the UV lights, a stepwise increase in the ratio was observed and reached the

337 maximum value of 1.60 at t=1.1 h as a result of the second-generation oxidation chemistry. After

338 that, the ratio kept decreasing. A small bump was observed after the second introduction of OH

339 and then the ratio kept decreasing. One possible explanation for this continuous decrease is the

340 effect of the size-dependent particle wall-loss process. The faster removal of smaller particles

341 (which contain more SOA than sulfate) than that of the bigger ones (which have a lower SOA to

342 sulfate ratio) can lead to a decrease of the overall organic to sulfate ratio. Fig. 7 shows the size

343 dependence of the Org/Sulf, together with the mass distribution of both organic and sulfate for

344 Exp. 1. The Org/Sulf decreased dramatically from 10 to 1 over the particle vacuum aerodynamic

345 diameter (D_{va}) range of 200 – 500 nm, indicating strong composition dependence on particle size.

346 Since the majority of the mass is distributed in this range, the size-dependent particle wall-loss rate

347 can contribute significantly to the decrease observed in Fig. 6 after the Org/Sulf reached its

348 maximum.

349

350 **4.1 Effect of size-dependent losses on the organic to sulfate ratio**

351 To quantify the effect of the size-dependence of the particle wall-loss process on the

352 organic to sulfate ratio, we discretized the AMS-measured mass distribution $M(D_p)$ into 10 bins

353 in the particle diameter space and defined a mass-weighted particle wall-loss rate constant for each

354 species j, $\bar{k}_j$, as

355

$$\bar{k}_j = \sum_{i=1}^{10} M_{ij} k_i / \sum_{i=1}^{10} M_{ij} \tag{4}$$

357

358 where M_{ij} is the aerosol mass concentration of species j for size bin i and k_i is the averaged $k(D_p)$

359 across size bin i. Note that the particle diameter used in this section refers to the SMPS-measured

360 mobility equivalent diameter D_p. The particle vacuum aerodynamic diameters derived from the

361 AMS measurements have been converted to D_p using an SOA density of 1.4 µg m^{-3}.

362 From Eqn. 4 we are able to determine a mass-weighted particle wall-loss rate constant for

363 sulfate, $\bar{k}_{SO_4}$, and for organics, $\bar{k}_{Org}$. For the period after completion of the reactions and if there

364 are only particle losses to the walls the Org/Sulf ratio should satisfy:

365

$$(\text{Org/Sulf})(t) = (\text{Org/Sulf})_m(t) \exp(\bar{k}_{SO_4} - \bar{k}_{Org}) t \tag{5}$$

where $(\mathrm{Org/Sulf})_m(t)$ is the AMS-measured and $(\mathrm{Org/Sulf})(t)$ the loss-corrected organic to sulfate ratio.

We can test if indeed the particle wall losses are responsible for the decreasing ratio in Exp. 1 focusing on the period from $t_1 = 1.2\,\mathrm{h}$ to $t_2 = 1.7\,\mathrm{h}$ (Fig. 6). In this example t_1 corresponds to the maximum Org/Sulf and t_2 is the second time in which the UV lights were turned on. Applying Eqn. 4, we found the mass-weighted particle wall-loss rate constant for organics, $\bar{k}_{Org} = 0.06\,h^{-1}$, and for sulfate, $\bar{k}_{SO_4} = 0.05\,h^{-1}$. The black line in the inset graph of Fig. 6 indicates the particle wall-loss corrected Org/Sulf for the chosen time period using Eqn. 5. The loss-corrected ratio remained relatively constant indicating that the size-dependent particle wall-loss process coupled with the different size distributions of the sulfate and organics were causing the decrease in the ratio. This exercise was repeated for the other experiments arriving in the same conclusion.

4.2 Effect of chemical aging on additional SOA formation

To quantify aging effects based on the SMPS measurements, we define the fractional change in the particle wall-loss corrected SOA mass concentration after aging, $\Delta[\mathrm{OA}]$, as:

$$\Delta[\mathrm{OA}] = (C_{\mathrm{SOA},2} - C_{\mathrm{SOA,UV}})/C_{\mathrm{SOA},1}, \tag{6}$$

where $C_{\mathrm{SOA,UV}}$ is the particle wall-loss corrected aerosol mass concentration at the time when we first turned on the UV lights. $C_{\mathrm{SOA,\,UV}}$ can be equal to $C_{\mathrm{SOA},1}$ depending on how level the first-generation SOA mass concentration remains after wall-loss correction. Fig. 8 summarizes the $\Delta[\mathrm{OA}]$ for all five experiments with the values and corresponding errors listed in Table 2. The OH exposure resulted in an average increase of 24±6 % in SOA mass concentration after aging, ranging from 20 to 29 %. Our HONO injection method creates OH levels of about 2.4×10^7 molecules $\mathrm{cm^{-3}}$ for the first hour and then the concentration dropped to around 5×10^6 molecules $\mathrm{cm^{-3}}$. The OH exposure is equivalent to 2-4 days of typical atmospheric oxidation conditions, assuming an OH concentration of 2×10^6 molecules $\mathrm{cm^{-3}}$. The uncertainties displayed in Fig. 8 were propagated from uncertainties in the SOA mass concentration.

To quantify aging effects based on the AMS data, we define the fractional change in the organic to sulfate ratio:

398

$$\Delta[Org/Sulf] = ([Org/Sulf]_2 - [Org/Sulf]_{UV})/[Org/Sulf]_1, \qquad (7)$$

400

where $[Org/Sulf]_{UV}$ refers to the organic to sulfate ratio at the time when we first turned on the UV lights, $[Org/Sulf]_1$ the maximum before we first turned on the UV lights and $[Org/Sulf]_2$ the maximum after the OH exposure. Fig. 8 summarizes the $\Delta[Org/Sulf]$ calculated for all five experiments with the values and corresponding errors listed in Table 2. The uncertainties are based on the deviation between the measured and the corrected Org/Sulf (Fig. 6 inset) over the chosen time period. An associated error is calculated respectively for $[Org/Sulf]_{UV}$, $[Org/Sulf]_1$ and $[Org/Sulf]_2$. The reported error for $\Delta[Org/Sulf]$ in Table 2 is the propagated results of the three. For experiments in this work, the percent increase in organic to sulfate ratios ranged from 18 to 27 % with an average increase of 21±4 %. The values are fairly consistent with the SMPS-derived $\Delta[OA]$.

4.2.1 Role of RH

Exp. 5, performed at the intermediate RH of 50 %, resulted in a comparable change in SOA formation after aging as experiments at lower RH (Fig. 8). In this experiment, the increase in Org/Sulf after aging was 21.2 %, 1.5 % higher than the average $\Delta[Org/Sulf]$ of experiments 2-4. $\Delta[OA]$ for Exp. 5 was 20.5 %, about 2 % lower than the average $\Delta[OA]$ of experiments 2-4. The effect of RH on the SOA formation during chemical aging, at least for these conditions, appears to be small.

4.2.2 Role of organic vapor loss to the Teflon walls

For chamber SOA experiments with preexisting particles, the particles act as competing surface against the chamber walls. We calculated the condensation sink (CS) of particles using the method described in Trump et al. (2014) with a unit accommodation coefficient, consistent with recent findings (Julin et al., 2014; Palm et al., 2016). The calculated condensation sink in the form of time scale for vapors condensing onto particles (1/CS) for Exp. 1 is shown in Fig. 9. During the entire experiment, the timescale for vapors to condense onto particles remained less than a minute. Compared to the organic vapor wall-loss timescale of 15 min in the CMU chamber (Ye et al., 2016), the vapors condense onto the particles 15 times faster than that onto the walls. This

429 corresponds to a 6.3 % loss of the semi-volatile vapors to the walls. Assuming the yields for the

430 experiments conducted in this work also increase by 6.3 %, the absolute yields should be increased

431 by 1-3 % after accounting for the vapor wall-loss effect. This approach is a conservative estimation

432 of vapor wall loss, and yet the results are consistent with what we observed from the measurements.

433 As indicated in Fig. 6, the organic to sulfate ratio stayed practically constant after its first peak at

434 t=0.7 h until the introduction of OH. This is consistent with the fact that the semi-volatiles formed

435 in our system only accounted for a small fraction of the products. Ye et al. (2016) studied the

436 SVOCs formed in the α-pinene ozonolysis system and found 20 % SVOCs in the products formed

437 from experiments with moderate precursor concentration (α-pinene=75 ppb). They also observed

438 that the SVOC fraction increased with increased amounts of reacted α-pinene. Since the reacted

439 α-pinene in our experiments was less than 35 ppb, our observation of small amount of SVOCs

440 forming is also consistent with their results.

441 The situation is a little more complex for the second-generation oxidation because material

442 with higher volatilities that could have become SOA were lost during the time after the end of the

443 first phase and before the beginning of the second. To address this issue, OH radicals were

444 introduced about an hour earlier in Exp. 1 as compared to the rest of the experiments. A shorter

445 timescale ensures the first-generation vapor products react efficiently with OH instead of

446 interacting with the chamber walls as in the case of longer timescales. There was an increase of

447 27 % in Org/Sulf in this experiment after aging, 7 % more than the average of the other four

448 experiments. Δ[OA] for Exp. 1 was 29.4 %, about 7.5 % higher than the average of the rest four

449 experiments. If we attribute this 7 % difference purely to the vapor wall-loss effect, then we

450 estimate that vapor losses can increase the additional SOA formation by roughly another 10 % for

451 the experiments conducted in this work.

452

453 **4.3 Effect of chemical aging on aerosol composition**

454 Fig. 10 summarizes the absolute increase in O:C after the two doses of OH, respectively,

455 with the corresponding exposure required to achieve the increase. As we discussed above using

456 Exp. 1 as an example, the O:C in all experiments showed a stepwise increase after the first OH

457 introduction while it grew continuously after the second OH introduction until the end of the

458 experiment. For these five experiments, it took 10 - 30 min for the O:C to increase by 0.02-0.04.

459 The stepwise increase in O:C is caused by the rapid reactions between the first generation vapor

460   products and the OH. One of the major products identified in the gas phase from the α-pinene

461   ozonolysis system, pinonaldehyde, reacts with OH at a rate of 3.5×10^{-11} cm^3 $molecule^{-1}$ s^{-1} (Davis

462   et al., 2007). During the first hour of OH introduction, the OH concentration remains on average

463   at a steady state of 2.4×10^7 molecule cm^{-3}. A quick estimation of $1/k_{OH}[OH]$ gives a timescale

464   of approximately 16 min, which is consistent with what we observed in these experiments.

465   The second exposure corresponds to the period until the end of each experiment. The

466   increase in O:C of 0.01 to 0.04 during this stage clearly indicates change in SOA composition,

467   however paired with minimum change in SOA mass. Although gas-phase reactions can contribute

468   to these observed changes in O:C, the corresponding condensation of the products should also

469   result in a detectable increase in SOA concentration during the same period. Given that changes

470   in SOA concentration could not be detected the contribution of gas-phase oxidation was probably

471   small. In addition, we observed small amounts of SVOCs forming in our system as discussed above.

472   The significant change in O:C without corresponding increase in SOA mass concentration was

473   likely caused by heterogeneous reactions.

474   Based on the HR family analysis results, the less oxidized ion family CH decreased around

475   10 percent during the aging process (i.e., from 41.9 to 38.1 percent of the OA in Exp. 1 and from

476   40.5 to 35.3 percent in Exp. 2) while the more oxidized CHO_2 increased 4 percent in Exp. 1 (from

477   12.8 to 13.3 percent) and 16 percent in Exp. 2 (from 14.9 to 17.3 percent). The changes in the

478   family CHO were +4 percent in Exp. 1 and -6 percent in Exp. 2, suggesting that there was both

479   production and destruction of the corresponding family members. The concentration of

480   organonitrates was, as expected, close to zero initially in these experiments. At the end of the aging

481   process, the NO family represented 3-3.5 % of the OA.

482   CO_2^+ (m/z 44) from family CHO_2 and $C_2H_3O^+$ (m/z 43) from family CHO are usually

483   identified in aged and relatively fresh aerosols, respectively. Their fractions of the total organics,

484   f_{44} and f_{43}, have been used as chemical indicators in chamber experiments (Donahue et al., 2012).

485   During the dark ozonolysis period of Exp. 1 (Fig. S2), the f_{43} increased initially and stayed

486   practically constant after t=0.2 h, while f_{44} decreased. After the first introduction of OH, both f_{43}

487   and f_{44} showed a stepwise increase. After the second introduction of OH, f_{43} decreased while f_{44}

488   increased over time until the end of the experiment, indicating that the SOA was getting

489   progressively more oxidized during aging. During Exp. 2 (Fig. S4), f_{43} increased sharply initially

490   and then slowly decreased during the dark ozonolysis period. This is consistent with the "ripening"

491   effect observed during the MUCHACHAS campaign (Donahue et al., 2012). Overall, f_{43}

492   decreased while f_{44} increased over the course of Exp. 2, indicating that the initially formed SOA

493   was getting more oxidized during aging.

494

495   **4.4 Comparison with other studies**

496   Overall, the results from our chamber experiments in this work are consistent to those from

497   the MUCHACHAS chambers. After adopting a size-dependent particle wall-loss correction

498   method, we observed 20-30 % additional SOA formation after aging. Vapor wall-loss effect can

499   account for an additional 10 %, increasing the range to 20-40 %. The O:C presented a stepwise

500   increase of 0.02-0.04 after the first introduction of OH, and then increased gradually overtime after

501   the second introduction of OH.

502   During the MUCHACHAS campaign, mixtures of SOA and gas-phase products formed in

503   the Paul Scherrer Institute (PSI) 27 m^3 Teflon chamber from low (10 ppb) and high (40 ppb) initial

504   α-pinene concentration were exposed to OH by TME ozonolysis and HONO photolysis at an RH

505   of approximately 50 % (Tritscher et al. 2011). An OH concentration of 2×10^6 to 10×10^6 molecules

506   cm^{-3} was maintained up to four hours. The authors reported an additional 50 % SOA mass forming

507   after aging using the first-order, size-independent particle wall-loss correction for the suspended

508   organic mass concentration measured by AMS. An increase of 0.04 in the oxygen to carbon ratio

509   was also observed during aging.

510   In the 84.5 m^3 Aerosol Interaction and Dynamics in the Atmosphere (AIDA) aluminum

511   chamber at Karlsruhe Institute of Technology, an OH concentration of 2×10^6 to 10×10^6 molecules

512   cm^{-3} was used by a constant flow of TME (dark aging). The authors observed an increase of 17-

513   55 % in the SMPS-derived SOA mass concentration (density corrected) after aging during four

514   experiments with initial α-pinene concentration ranging from 14 to 56 ppb (Salo et al., 2011). In

515   the 270 m^3 Simulation of Atmospheric Photochemistry in a large Reaction (SAPHIR) Teflon

516   chamber at Forchungzentrum Jülich, SOA and vapors generated from the ozonolysis of 40 ppb α-

517   pinene was aged for three consecutive days with OH produced by ambient light chemistry. An OH

518   concentration of $2\text{-}5\times10^6$ molecules cm^{-3} was maintained and 9 %, 4 % and 1 % additional SOA

519   was formed respectively after aging each day. These values were corrected for particle wall loss

520   using different wall-loss rate constants determined during different periods of the experiment.

521   Our result of 20-40 % additional SOA formation due to aging is well within the range of

522 that from the above chambers. The difference in the results from each chamber could potentially

523 be attributed to different OH exposure (e.g. a constant flow of HONO or TME was provided in the

524 PSI chamber). Other plausible explanations include whether the reported values were particle wall-

525 loss corrected and whether the same method was adopted for the correction.

526   For the HONO aging experiment performed in the CMU chamber during the

527 MUCHACHAS campaign, Henry and Donahue (2012) suggested a potentially strong photolysis

528 effect based on decreasing organic to sulfate ratio derived from the AMS measurements. In our

529 experiments, the organic to sulfate ratio was affected by the size-dependent wall-loss process. Both

530 the AMS-measured organic to sulfate ratio and the SMPS-measured OA remained relatively

531 constant after correcting for the size dependence of the particle-wall process in these experiments.

532 We thus conclude that minimum photolysis was observed for our experiments.

533

534 5. Conclusions

535   With an OH exposure equivalent to 2-4 days of typical atmospheric oxidation conditions,

536 the OH aging of the α-pinene ozonolysis products formed 20-40 % additional SOA mass for the

537 experimental conditions used in this work. Elevated RH up to 50 % has minimum effect on SOA

538 production due to aging. We have constrained the aging effects on additional SOA formation

539 quantitatively using both SMPS and AMS measurements.

540   A more oxygenated product distribution was observed after aging. A stepwise increase of

541 0.02-0.04 in O:C was observed within half an hour after the first introduction of OH. After the

542 second-generation products were exposed to additional OH, the O:C grew continuously until the

543 end of the experiments with an absolute increase of up to 0.04. During this period, minimum SOA

544 production was observed. We attribute this phenomenon to condensed-phase reactions. Further

545 investigation on a molecular scale is needed.

546   This work explored the additional SOA formation potential of the α-pinene ozonolysis

547 products under high NO_x conditions. The aging time scale of this study of a few days corresponds

548 to the atmospheric lifetime of the corresponding aerosol. The additional formation of SOA

549 observed here is clearly non-negligible, but is also much less than the doubling or tripling of the

550 SOA that has been assumed in few modeling studies (Lane et al., 2008) which resulted in

551 overprediction of the biogenic SOA. The present results can be used for the improvements of the

552 currently used parameterizations for the aging of a-pinene SOA products in CTMs.

553

554 *Acknowledgement:* The work was funded by the EPA STAR grant 835405 and the EUROCHAMP-

555 2020 EU project.

556

557 6. References

558 Barmet, P., Dommen, J., DeCarlo, P. F., Tritscher, T., Praplan, A. P., Platt, S. M., Prévôt A. S. H.,
559 Donahue, N. M., and Baltensperger, U.: OH clock determination by proton transfer
560 reaction mass spectrometry at an environmental chamber, Atmos. Meas. Tech., 5, 647–656,
561 2012.

562 Canagaratna, M. R., Jimenez, J. L., Kroll, J. H., Chen, Q., Kessler, S. H., Massoli, P., Hildebrandt
563 Ruiz, L., Fortner, E., Williams, L. R., Wilson, K. R., Surratt, J. D., Donahue, N. M., Jayne,
564 J. T., and Worsnop, D. R.: Elemental ratio measurements of organic compounds using
565 aerosol mass spectrometry: characterization, improved calibration, and implications,
566 Atmos. Chem. Phys., 15, 253-272, 2015.

567 Chacon-Madrid, H. J., Henry, K. M., and Donahue, N. M.: Photo-oxidation of pinonaldehyde at
568 low NO_x: from chemistry to organic aerosol formation, Atmos. Chem. Phys., 13, 3227-
569 3236, 2013.

570 Cocker III, D. R., Flagan, R. C., and Seinfeld, J. H.: State-of-the-art chamber facility for studying
571 atmospheric aerosol chemistry, Environ. Sci. Technol., 35, 2594–2601, 2001.

572 Crump, J. G., and Seinfeld, J. H.: Turbulent deposition and gravitational sedimentation of an
573 aerosol in a vessel of arbitrary shape, J. Aerosol Sci., 2, 405–415, 1981.

574 Davidson, C. I., Phalen, R. F., and Solomon, P. A.: Airborne particulate matter and human health:
575 a review, Aerosol Sci. Technol, 39, 737–749, 2005.

576 Davis, M. E., Talukdar, R. K., Notte, G., Ellison, G. B., Burkholder, J. B.: Rate coefficients for
577 the OH+Pinonaldehyde ($C_{10}H_{16}O_2$) reaction between 297 and 374 K, Environ. Sci.
578 Technol., 41, 3959-3965, 2007.

579 Donahue, N. M., Henry, K. M., Mentel, T. F., Kiendler-Scharr, A., Spindler, C., Bohn, B., Brauers,
580 T., Dorn, H. P., Fuchs, H., Tillmann, R., Wahner, A., Saathoff, H., Naumann, K.-H.,
581 Mohler, O., Leisner, T., Muller, L., Reinnig, M.-C., Hoffmann, T., Salo, K., Hallquist, M.,
582 Frosch, M., Bilde, M., Tritscher, T., Barmet, P., Praplan, A. P., DeCarlo, P. F., Dommen,
583 J., Prevot, A. S. H., and Baltensperger, U.: Aging of biogenic secondary organic aerosol
584 via gas-phase OH radical reactions, Proc. Natl. Acad. Sci., U.S.A., 109, 13503 −13508,
585 2012.

586 Donahue, N. M., Robinson, A. L., Stanier, C. O., and Pandis, S. N.: Coupled partitioning, dilution
587 and chemical aging of semivolatile organics, Environ. Sci. Technol., 40, 2635-2643, 2006.

588 George, I. J., Slowik J., and Abbatt J. P. D.: Chemical aging of ambient organic aerosol from
589 heterogeneous reaction with hydroxyl radicals, Geophys. Res. Lett., 35, L13811, 2008.

590 Griffin, R. J., Cocker, D. R., Seinfeld, J. H., and Dabdub, D.: Estimate of global atmospheric
591 organic aerosol from oxidation of biogenic hydrocarbons, Geophys. Res. Lett., 26, 2721–
592 2724, 1999.

Grosjean. D., and Seinfeld, J. H.: Parameterization of the formation potential of secondary organic aerosols, Atmos. Environ., 23, 1733-1747, 1989.

Henry, K. M., and Donahue, N. M.: Photochemical aging of α-pinene secondary organic aerosol: effects of OH radical sources and photolysis: J. Phys. Chem. A, 116, 5932−5940, 2012.

Henry, K. M., Lohaus T., and Donahue, N. M.: Organic aerosol yields from α-pinene oxidation: bridging the gap between first-generation yields and aging chemistry, Environ. Sci. Technol., 46, 12347−12354, 2012.

Intergovernmental Panel on Climate Change: Climate Change 2007: Synthesis Report. Contribution of Working Groups I, II and III to the Fourth Assessment Report of the Intergovernmental Panel on Climate Change, edited by R. K. Pachauri and A. Reisinger, eds., 104 pp., Cambridge Univ. Press, New York, 2007.

Izumi, K., and Fukyama, T.: Photochemical aerosol formation from aromatic hydrocarbons in the presence of NOx, Atmos. Environ., 24A, 1433-1441, 1990.

Julin, J., Winkler, P. M., Donahue, N. M., Wagner, P. E., and Riipinen, I.: Near-unity mass accommodation coefficient of organic molecules of varying structure, Environ. Sci. Technol., 48, 12083–12089, 2014.

Kalberer, M., Sax, M., and Samburova, V.: Molecular size evolution of oligomers in organic aerosols collected in urban atmospheres and generated in a smog chamber, Environ. Sci. Technol., 40, 5917−5922, 2006.

Keywood, M. D., Varutbangkul, V., Bahreini, R., Flagan, R. C., and Seinfeld, J. H.: Secondary organic aerosol formation from the ozonolysis of cycloalkenes and related compounds, Environ. Sci. Technol., 38, 4157–4164, 2004.

Krechmer, J. E., Pagonis, D., Ziemann, P. J., and Jimenez, J. L.: Quantification of gas-wall partitioning in Teflon environmental chambers using rapid bursts of low-volatility oxidized species generated in situ, Environ. Sci. Technol., 50, 5757–5765, 2016.

Kostenidou E., Pathak R. K., and Pandis S. N.: An algorithm for the calculation of secondary organic aerosol density combining AMS and SMPS data; Aerosol Sci. Technol., 41, 1002–1010, 2007.

Kuwata, M., Zorn S. R., and Martin S. T.: Using elemental ratios to predict the density of organic material composed of carbon, hydrogen, and oxygen, Environ. Sci. Technol., 46, 787-794, 2012.Lambe, A. T., Miracolo, M. A., Hennigan, C. J., Robinson, A. L., and Donahue, N. M.: Effective rate constants and uptake coefficients for the reactions of organic molecular markers (n-alkanes, hopanes and steranes) in motor oil and diesel primary organic aerosols with hydroxyl radicals, Environ. Sci. Technol., 43, 8794−8800, 2009.

Lane, T., Donahue, N. M., and Pandis, S. N.: Simulating secondary organic aerosol formation using the volatility basis-set approach in a chemical transport model, Atmos. Environ., 42, 7439-7451, 2008.

Loza, C. L., Chhabra, P. S., Yee, L. D., Craven, J. S., Flagan, R. C., and Seinfeld, J. H.: Chemical aging of m-xylene secondary organic aerosol: laboratory chamber study, Atmos. Chem. Phys., 12, 151–167, 2012.

Matsunaga, A., and Ziemann, P. J.: Gas-wall partitioning of organic compounds in a Teflon film chamber and potential effects on reaction product and aerosol yield measurements, Aerosol Sci. Technol., 44, 881–892, 2010.

McMurry, P. H., and Rader, D. J.: Aerosol wall losses in electrically charged chambers, Atmos. Chem. Phys., 4, 249–268, 1985.

Müller, L., Reinnig, M. C., Naumann, K. H., Saathoff, H., Mentel, T. F., Donahue, N. M., and Hoffmann, T.: Formation of 3-methyl-1,2,3-butanetricarboxylic acid via gas phase oxidation of pinonic acid - a mass spectrometric study of SOA aging, Atmos. Chem. Phys., 12, 1483–1496, 2012.

Nah, T., McVay, R. C., Zhang, X., Boyd, C. M., Seinfeld, J. H., and Ng, N. L.: Influence of seed aerosol surface area and oxidation rate on vapor wall deposition and SOA mass yields: a case study with α-pinene ozonolysis, Atmos. Chem. Phys., 16, 9361–9379, 2016.

Ng, N. L., Kroll, J. H., Chan, A. W. H., Chhabra, P. S., Flagan, R. C., and Seinfeld, J. H.: Secondary organic aerosol formation from m -xylene, toluene, and benzene, Atmos. Chem. Phys., 7, 3909–3922, 2007.

Odum J. R., Hoffmann, T., Bowman, F., Collins, T., Flagan, R. C., and Seinfeld, J. H.: Gas-particle partitioning and secondary organic aerosol yields, Environ. Sci. Technol., 30, 2580-2585, 1996.

Palm, B. B., Campuzano-Jost, P., Ortega, A. M., Day, D. A., Kaser, L., Jud, W., Karl, T., Hansel, A., Hunter, J. F., Cross, E. S., Kroll, J. H., Peng, Z., Brune, W. H., and Jimenez, J. L.: In situ secondary organic aerosol formation from ambient pine forest air using an oxidation flow reactor, Atmos. Chem. Phys., 16, 2943–2970, 2016.

Paulson, S. E., Chung, M., Sen, A. D., and Orzechowska, G.: Measurement of OH radical formation from the reaction of ozone with several biogenic alkenes, J. Geophys. Res., 103, 25533-25539, 1998.

Pope, C. A., Ezzati, M., and Dockery, D. W.: Fine-particulate air pollution and life expectancy in the United States, New Engl. J. Med., 360, 376-386, 2009.

Qi, L., Nakao, S., and Cocker, D. R.: Aging of secondary organic aerosol from α-pinene ozonolysis: Roles of hydroxyl and nitrate radicals, J. Air & Waste Manag. Assoc., 62, 1359–1369, 2012.

Robinson, A. L., Donahue, N. M., Shrivastava, M. K., Weitkamp, E. A., Sage, A. M., Grieshop, A. P., Lane, T. E., Pierce, J. R., and Pandis, S. N.: Rethinking organic aerosol: semivolatile emissions and photochemical aging, Science, 315, 1259–1262, 2007.

Salo, K., Hallquist, M., Jonsson, Å. M., Saathoff, H., Naumann, K.-H., Spindler, C., Tillmann R., Fuchs, H., Bohn, B.; Rubach, F., Mentel, T. F., Müller, L., Reinnig, M., Hoffmann, T., and Donahue, N. M.: Volatility of secondary organic aerosol during OH radical induced ageing; Atmos. Chem. Phys., 11, 11055–11067, 2011.

Tritscher, T., Dommen, J., DeCarlo, P. F., Gysel, M., Barmet, P. B., Praplan, A. P., Weingartner E., Prévôt, A. S. H., Riipinen, I., Donahue, N. M., and Baltensperger, U.: Volatility and hygroscopicity of aging secondary organic aerosol in a smog chamber, Atmos. Chem. Phys., 11, 11477–11496, 2011.

Trump, E. R., Riipinen, I., and Donahue, N. M.; Interactions between atmospheric ultrafine particles and secondary organic aerosol mass: a model study, Boreal Environ. Res., 19, 352–362, 2014

Tsimpidi, A. P., Karydis, V. A., Zavala, M., Lei, W., Bei, N., Molina, L., and Pandis, S. N.: Sources and production of organic aerosol in Mexico City: insights from the combination of a chemical transport model (PMCAMx-2008) and measurements during MILAGRO, Atmos. Chem. Phys., 11, 5153−5168, 2011.

Wang, N., Donahue, N. M., and Pandis, S.N.: Performance of different particle wall-loss correction methods for aging experiments of alpha-pinene SOA in a smog chamber, Aerosol Science and Technology; in preparation.

684   Ye, P., Ding, X., Hakala, J., Hofbauer, V., Robinson, E. S., and Donahue, N. M.: Vapor wall loss
685   of semi-volatile organic compounds in a Teflon chamber, Aerosol Science and Technology,
686   50, 822-834, 2016.
687   Ye, P., Ding, X., Ye, Q., and Robinson, E. S.: Uptake of semivolatile secondary organic aerosol
688   formed from α-pinene into nonvolatile polyethylene glycol probe particles, J. Phys. Chem.
689   A, 120, 1459-1467, 2016.
690   Zhang, Q., Jimenez, J. L., Canagaratna, M. R., Allan, J. D., Coe, H., Ulbrich, I., Alfarra, M. R.,
691   Takami, A., Middlebrook, A. M., Sun, Y. L., Dzepina, K., Dunlea, E., Docherty, K., De-
692   Carlo, P. F., Salcedo, D., Onasch, T., Jayne, J. T., Miyoshi, T., Shimono, A., Hatakeyama,
693   S., Takegawa, N., Kondo, Y., Schneider, J., Drewnick, F., Borrmann, S., Weimer, S.,
694   Demerjian, K., Williams, P., Bower, K., Bahreini, R., Cottrell, L., Griffin, R. J., Rautiainen,
695   J., Sun, J. Y., Zhang, Y. M., and Worsnop, D. R.: Ubiquity and dominance of oxygenated
696   species in organic aerosols in anthropogenically-influenced Northern Hemisphere
697   midlatitudes, Geophys. Res. Lett., 34, L13801, 2007.
698   Zhang, X., Cappa, D. C., Jathar, S. H., McVay, R. C., Ensberg, J. J., Kleeman, M. J., and Seinfeld,
699   J. H.: Influence of vapor wall loss in laboratory chambers on yields of secondary organic
700   aerosol, Proc. Natl. Acad. Sci., U.S.A., 111, 5802-5807, 2014.
701
702
703

704

705

706

707

Table 1: Initial conditions of the α-pinene ozonolysis aging experiments.

Experiment	α-pinene (ppb)	O$_3$ (ppb)	Initial seed surface area (μm^2 cm^{-3})	RH (%)	OH[a] ($\times 10^7$ molecules cm^{-3})	OH introduction time (h after α-pinene consumption)
1	33	450	850	<20	2.4	0.3
2	14	600	760	<20	2.7	0.8
3	35	450	720	<20	2.0	1.1
4	16	500	950	<20	2.4[b]	1.1
5	20	400	710	~50	2.7	0.8

[a]The OH concentration was calculated using the decay of butanol-d9 (monitored by PTRMS) (Barmet et al., 2012).

[b]Estimated OH concentration for Exp. 4 based on the other experiments. The PTRMS data was not available during that time for Exp. 4.

733

734

Table 2: SOA mass concentration and yields of the α-pinene ozonolysis aging experiments.

736

Experiment	$C_{SOA,1}$ (µg m^{-3})	Y_1 (%)	$C_{SOA,2}$ (µg m^{-3})	Y_2 (%)	ΔOA (%)	Δ[Org/Sulf] (%)
1	37.7±1.6	20.6±0.9	48.8±2.0	26.7±1.1	29.4±6.9	27.0±5.8
2	16.7±0.9	21.5±1.2	18.3±1.0	23.5±1.3	19.8±8.1	18.1±2.9
3	57.1±1.3	29.4±0.7	71.0±1.6	36.2±0.8	23.5±3.6	19.1±3.6
4	16.8±0.6	19.1±0.6	20.8±0.7	23.7±0.8	24.0±5.3	21.9±2.1
5	22.2±0.7	19.5±0.6	25.4±0.8	22.3±0.7	20.5±4.7	21.2±4.4

737

738

739

740

741

742

743

744
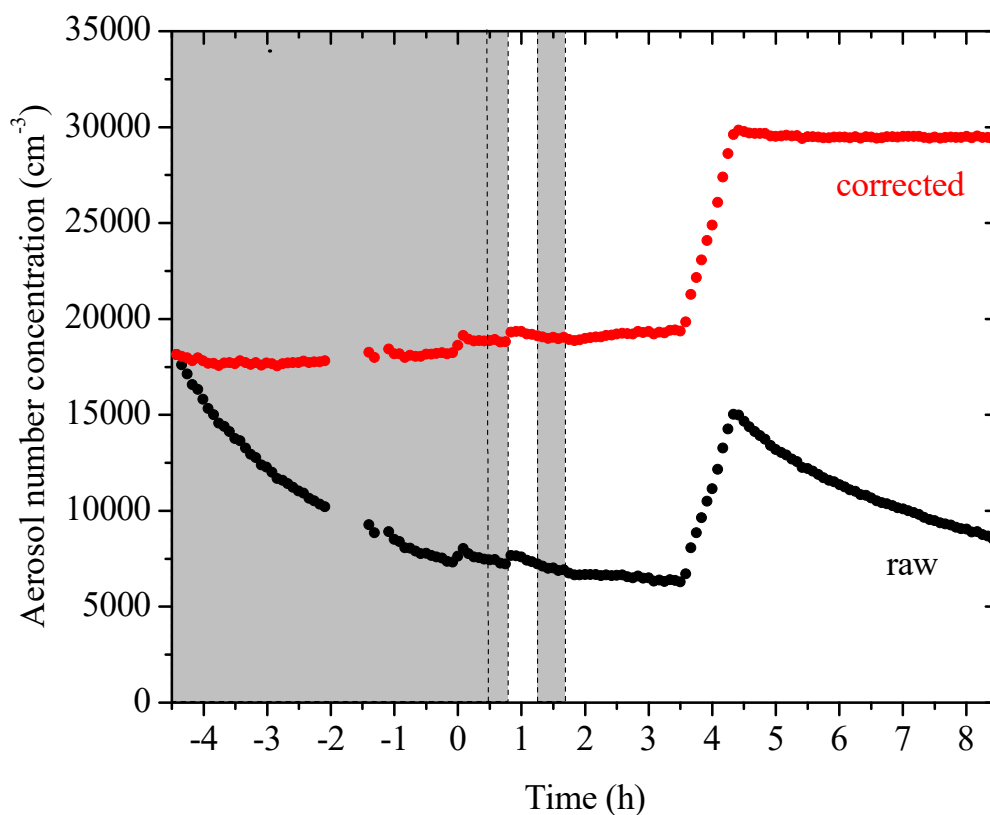
Figure 1: SMPS-measured (black symbols) and the size-dependent particle wall-loss corrected
(red symbols) aerosol number concentration evolution during a typical experiment (Exp. 1). Ozone
was added into the chamber at time zero to initiate α-pinene ozonolysis. The shaded areas indicate
that the chamber was dark. The dashed lines mark the beginning and the end of the two times
HONO were added, respectively. The increase in number concentration at t=3.5 h is due to the
injection of 5 g L^{-1} ammonium sulfate particles. An additional 100 cm^{-3} particles were formed due
to nucleation both at the ozonolysis step and the aging step. Data were not recorded from t=-2 h to
-1.4 h.

753

754

755
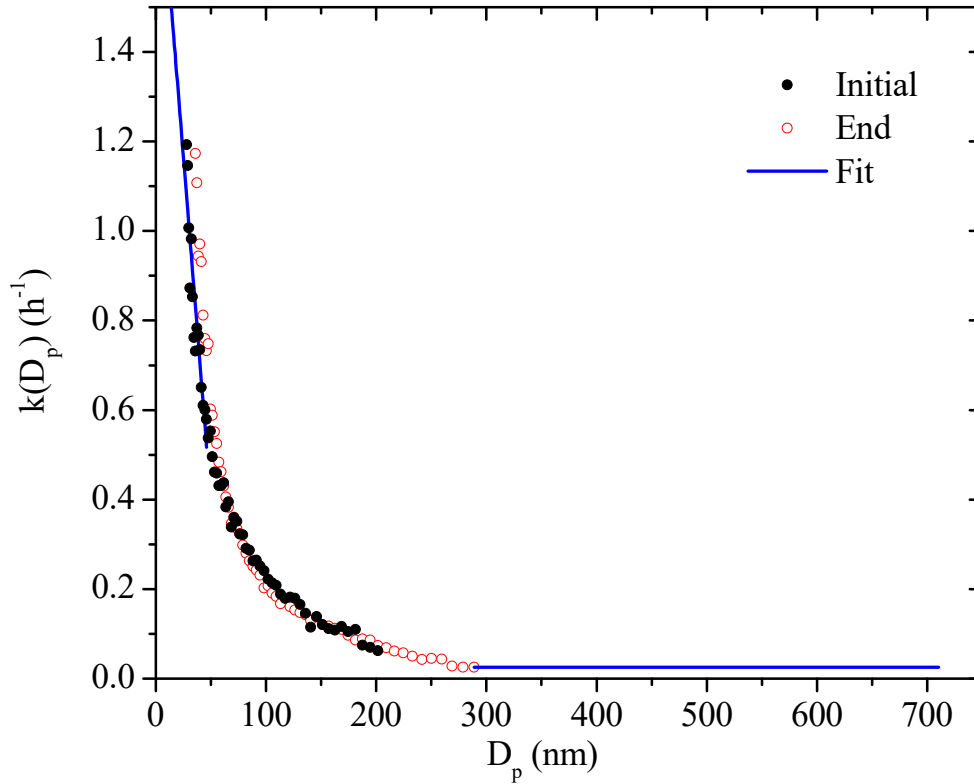
756
757 **Figure 2:** The size-dependent particle wall-loss rate constant profile, $k(D_p)$, for Exp. 1. The black
758 symbols are the rate constants calculated based on the wall-loss process of the initial ammonium
759 sulfate seed particles from $t=-4.5$ h to $t=0$ h, while the red open symbols those of the additional
760 ammonium sulfate particles at the end from $t=4.5$ h to $t=8.5$ h. The blue line is the fit determined.
761
762
763
764

765
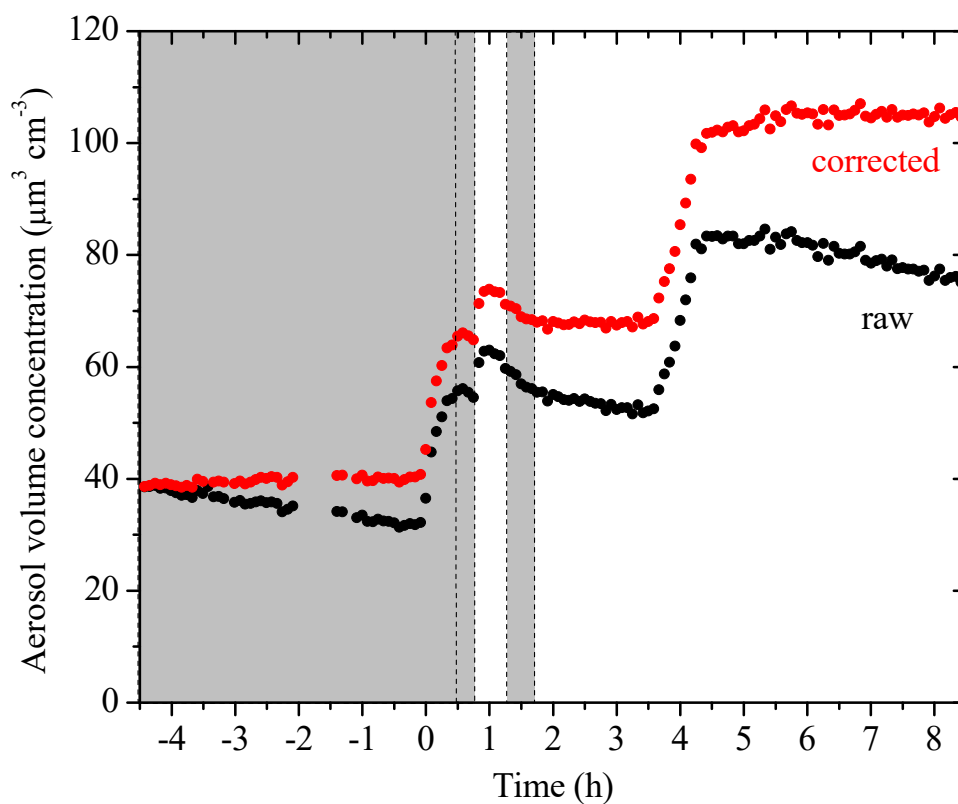
Figure 3: SMPS-measured (black symbols) and the size-dependent particle wall-loss corrected (red symbols) aerosol (seed and organic) volume concentration evolution during a typical experiment (Exp. 1). Ozone was added into the chamber at time zero to initiate α-pinene ozonolysis. The shaded areas indicate that the chamber was dark. The dashed lines mark the beginning and the end of the two times HONO were added, respectively. 5 g L^{-1} ammonium sulfate particles were injected into the chamber at t=3.5 h. Data were not recorded from t=-2 h to -1.4 h.

772
773
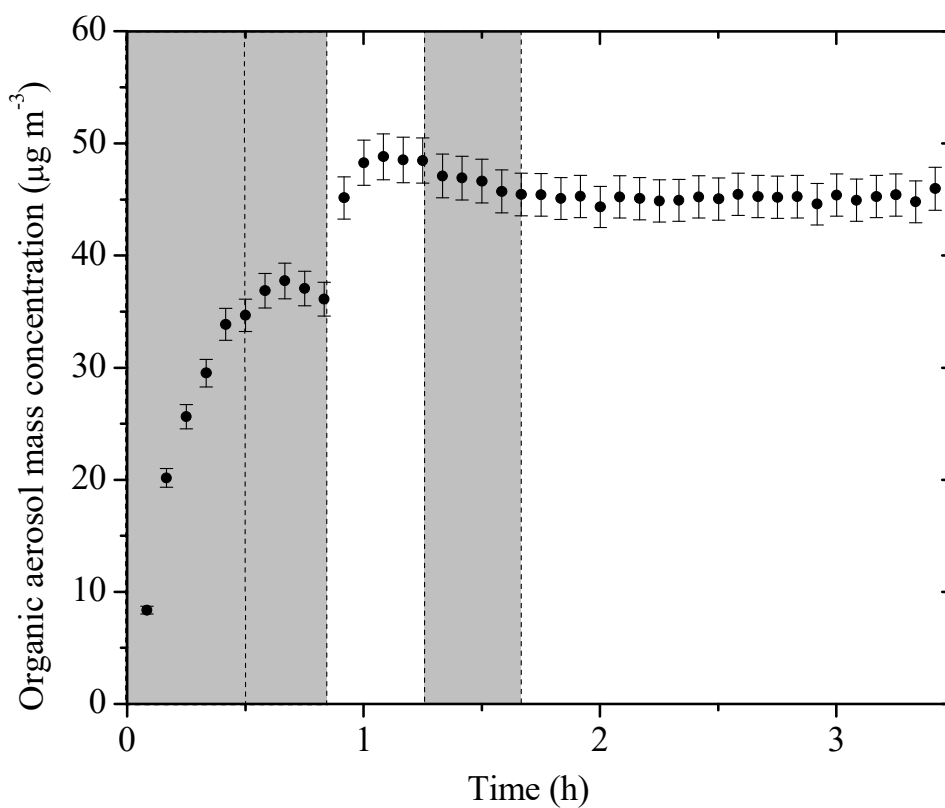
774
775
776 **Figure 4:** The particle wall-loss corrected SOA mass concentration (ρ=1.4 g cm^{-3}) evolution for
777 Exp. 1 derived from SMPS measurements. The corresponding error shown is due to the particle
778 wall-loss correction. Ozone was added into the chamber at time zero to initiate α-pinene ozonolysis.
779 The shaded areas indicate that the chamber was dark. The dashed lines mark the beginning and the
780 end of the two times HONO were added, respectively.
781

782
783
784

785
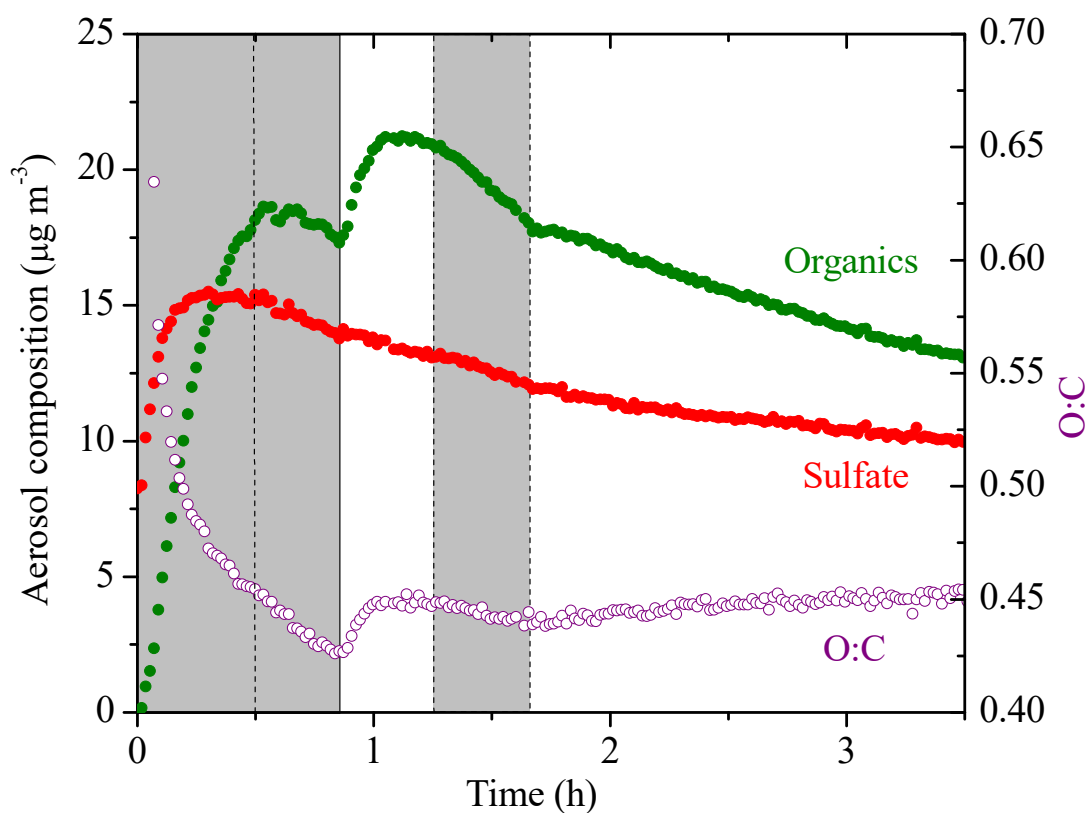
786
787 **Figure 5:** The AMS-measured aerosol composition (CE=1) (left axis) and the atomic oxygen to
788 carbon ratio (right axis) evolving with time for Exp. 4. The increase in the sulfate signal at t=0 is
789 the result of a change in the collection efficiency (CE). Ozone was added into the chamber at time
790 zero to initiate α-pinene ozonolysis. The shaded areas indicate that the chamber was dark. The
791 dashed lines mark the beginning and the end of the two times HONO were added, respectively.
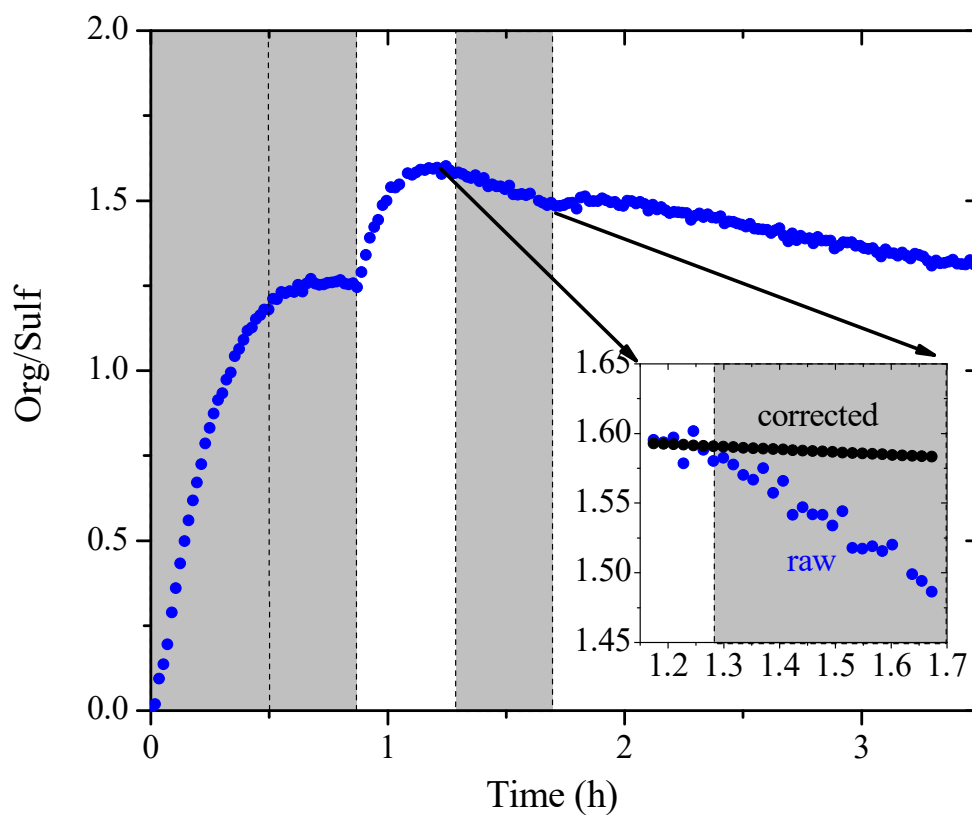
792

793 **Figure 6:** The AMS-derived organic to sulfate ratio time series for Exp. 1. The inset is a blow-up
794 of the Org/Sulf ratio from its maximum until the second time when the UV lights were turned on.
795 The black symbols are the particle wall-loss corrected Org/Sulf during that half hour. Ozone was
796 added into the chamber at time zero to initiate α-pinene ozonolysis. The shaded areas indicate that
797 the chamber was dark. The dashed lines mark the beginning and the end of the two times HONO
798 were added, respectively.

799
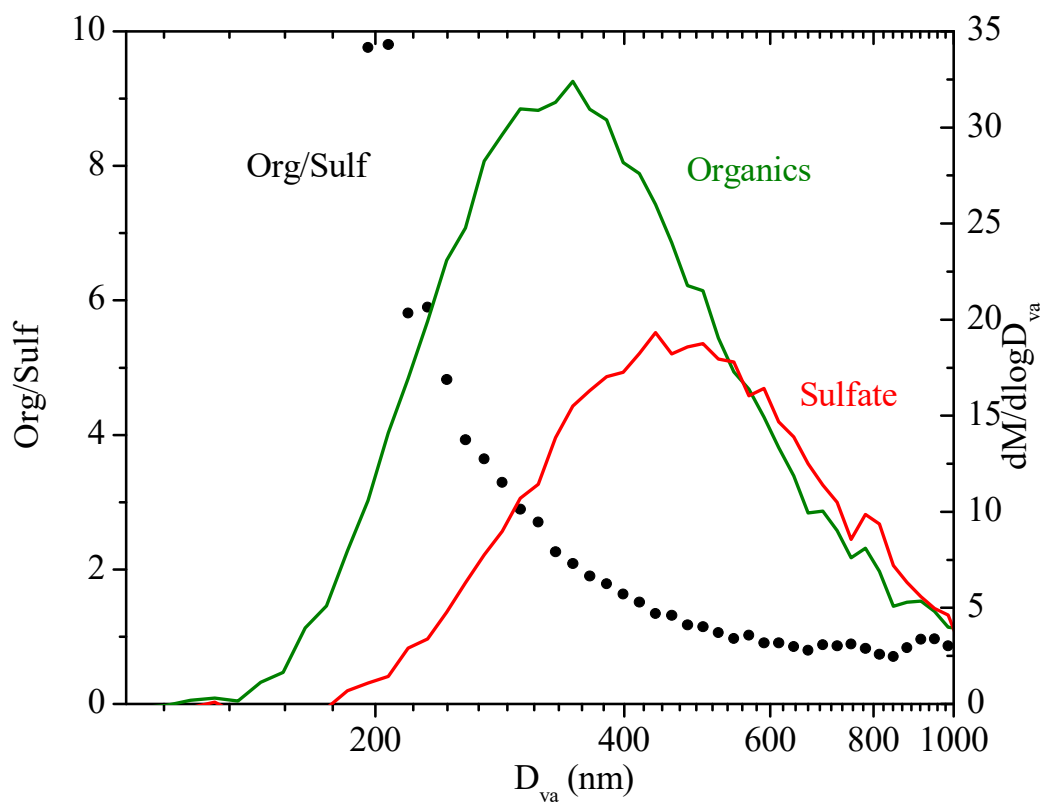
Figure 7: The dependence of the AMS-derived organic to sulfate ratio on particle vacuum
aerodynamic diameter for Exp. 1 (left axis). Also shown are the AMS-measured organic (green)
and sulfate (red) mass distribution (right axis). The results are based on PToF data averaged over
~2.5 hours (*t*=1.1 h to 3.5 h).

800
801
802
803
804
805
806
807
808
809
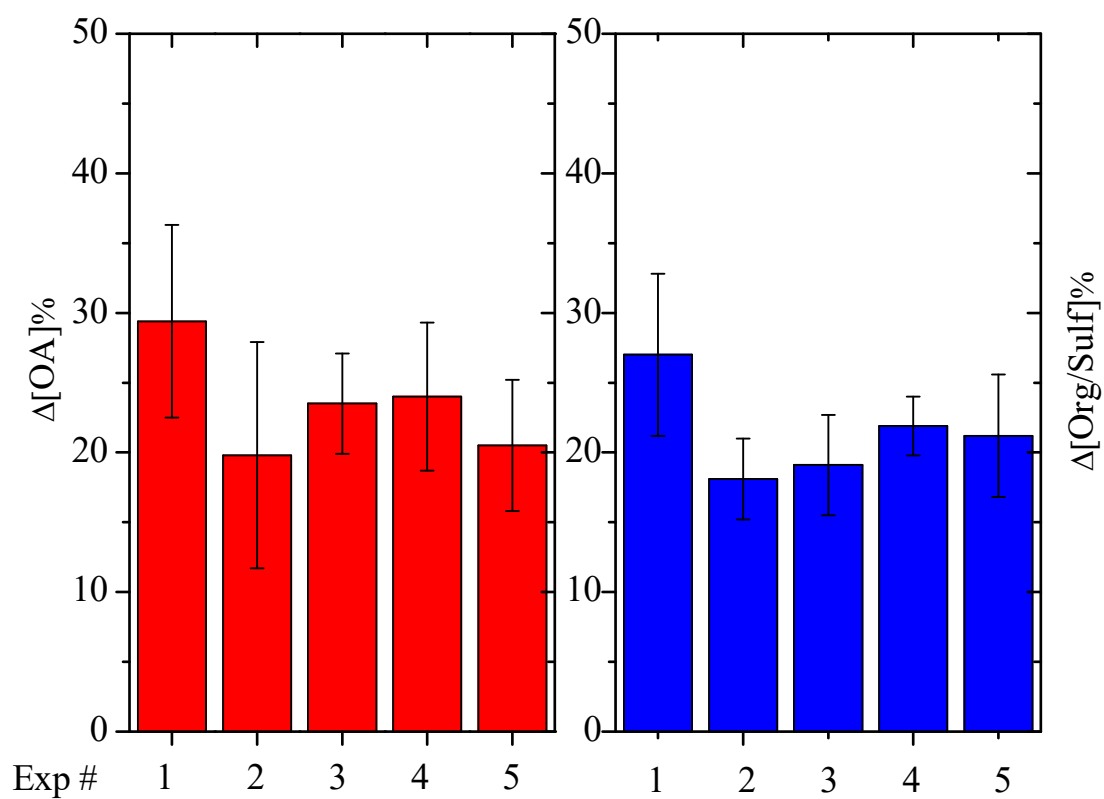
810

811

812 **Figure 8:** SMPS-derived percent change in the particle wall-loss corrected SOA (red columns)
813 mass concentration after aging and AMS-derived percent change in organic to sulfate ratio (blue
814 columns) after aging for all five experiments.

815

816

817

818

819

820

821
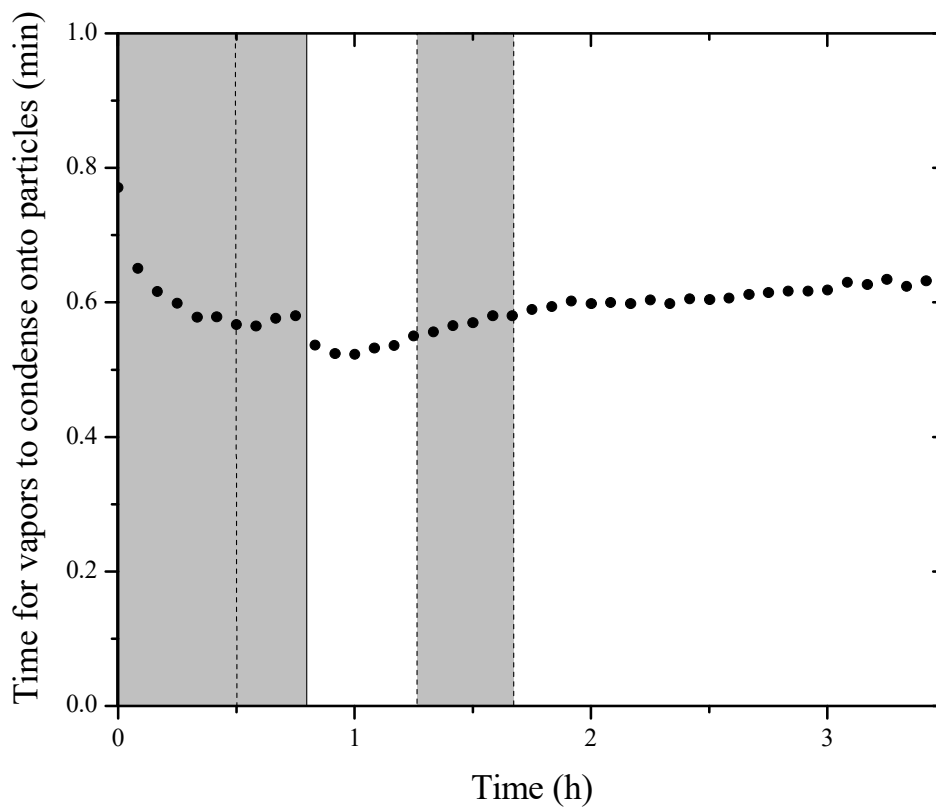
Figure 9: The calculated condensation sink (CS) in the form of time scale for vapors condensing onto particles (1/CS). Ozone was added into the chamber at time zero to initiate α-pinene ozonolysis. The shaded areas indicate that the chamber was dark. The dashed lines mark the beginning and the end of the two times HONO were added, respectively.
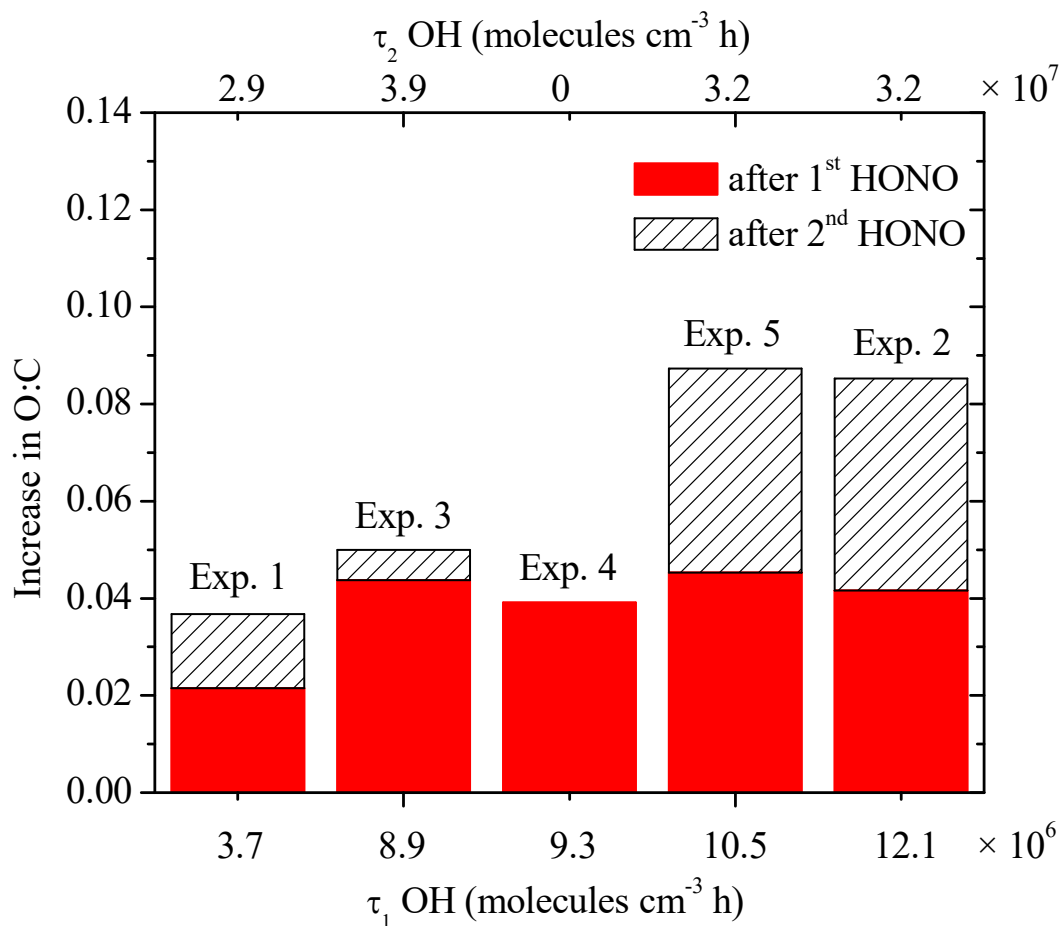
Figure 10: The absolute increase in O:C after the two doses of OH, respectively, with the corresponding exposure. The solid red columns are the increase in O:C after the first introduction of OH, with the corresponding exposure on the bottom axis. The hatched columns are the increase in O:C after the second introduction of OH, with the corresponding exposure on the top axis.